Peculiarities of dielectric losses in Fe_xO_y nanocomposite films

A.A. Evtukh[1,2*], A.I. Pylypov[2], Y.U. Muryi[1], O.V. Pylypova[2], S.V. Antonin[1], O.L. Bratus[1]

[1]*V. Lashkaryov Institute of Semiconductor Physics, NAS of Ukraine, 41 Nauky Ave., 03028 Kyiv, Ukraine*
[2]*Educational Scientific Institute of High Technologies, Taras Shevchenko National University of Kyiv, 4-g Hlushkova Avenue, Kyiv, Ukraine*
[*]*Corresponding author e-mail: anatoliy.evtukh@gmail.com*

Abstract. Dielectric losses are one of the main parameters of a dielectric. Generally, for many applications, they should be as low as possible; however, in the case of electromagnetic wave absorption, they should be high. This paper presents the results of the study on dielectric losses in Fe_xO_y nanocomposite films, which were investigated within a frequency range of 5 kHz to 5 MHz. It was demonstrated that the dielectric losses due to the applied AC signal decrease with frequency and increase with voltage. The analysis of the mechanisms of dielectric losses revealed that they are primarily caused by polarization. Dielectric losses resulting from conductivity were approximately two orders of magnitude lower, although they increase significantly with increasing applied voltage. This behavior correlates with the dependence of specific conductivity on voltage. The dielectric loss tangent (tan δ) and the dielectric loss factor (the imaginary part of the dielectric constant, ε″) are higher for the initial film compared to the annealed one. This difference can be attributed to the transformation of the film structure and its ordering during high-temperature thermal annealing. Overall, dielectric losses within the investigated frequency range are mainly caused by relaxation (thermally activated) polarization, which is characteristic of disordered nanocomposite films.

Keywords: nanocomposite films, dielectric losses, polarization, frequency, voltage, ion-plasma deposition, annealing.

https://doi.org/10.15407/spqeo29.01.057
PACS 62.25.De, 73.61.-r, 77.22.Gm, 81.07.-b, 81.15.-z

Manuscript received 08.01.26; revised version received 24.02.26; accepted for publication 18.03.26; published online 25.03.26.

1. Introduction

Nowadays, dielectric materials, as core components of capacitors, are key to the development of new energy storage materials, which are widely used in micro-electronic components, memory devices, capacitors, and other applications [1–3]. The specific capacitance and dielectric losses are among the most important parameters of capacitors. The development and design of high-performance dielectric materials is a research topic of practical significance in the field of inorganic materials [4, 5].

High dielectric constant and relatively low dielectric loss are essential for enhancing the performance of capacitance-based devices [6, 7]. Dielectrics with high dielectric constants and low losses are very attractive for applications in nanoelectronics and as supercapacitors. Over the past few decades, a giant dielectric constant has been reported in several material systems, which can be classified as follows: (1) doped ferroelectric ceramics; (2) epitaxial ferroelectric heterostructures [8]; (3) perovskite-related oxides, such as $CaCu_3Ti_4O_{12}$ (CCTO) [9]; (4) non-ferroelectric transition-metal oxides, such as doped NiO [10] and TiO_2 [11]; (5) metal-doped ceramics or composites [3]; and (6) metal-polymer composites [12]. For example, a giant dielectric constant coupled with low dielectric loss was observed in La-modified $PbTiO_3$ (PLT) with A-site vacancies [3].

The composites containing metal and silicon nanoparticles in a dielectric matrix are under intensive investigation [13–17]. Giant dielectric constant values ($\sim 10^{10}$) have been obtained for the composite film composed of copper nanowires and amorphous SiO_2 [18]. Some composite materials demonstrate the appearance of negative capacitance [19, 20]. This unusual effect is promising for the use of composite materials in novel micro- and nanoelectronics devices.

The electrical properties of dielectric and nanocomposite materials, particularly dielectric loss, can significantly impact the performance of electronic

© V. Lashkaryov Institute of Semiconductor Physics of the NAS of Ukraine, 2026
© Publisher PH "Akademperiodyka" of the NAS of Ukraine, 2026

devices, with low dielectric loss (tan δ(ω)) being essential for optimal functionality [21 – 24]. Most dielectric materials experience a gradual increase in dielectric loss as the temperature rises. Extensive research has been conducted on the mechanism of dielectric loss. The contributions of conduction loss and polarization loss (including interface polarization, dipole polarization, and defect-induced polarization) to dielectric loss have been addressed in [25]. Significant progress has been made in the study of materials with low dielectric loss and their mechanisms. The classical Debye model and its extended models (the Cole–Cole model, the Davidson–Cole model, and the Havriliak–Negami model) successfully describe the dielectric loss behavior dominated by the polarization mechanism at low temperatures [12, 21, 23, 26]. However, when the dielectric material exhibits relatively high conductivity, the dielectric loss attributed to this conductivity cannot be ignored. Therefore, in analyzing the dielectric loss of nanocomposites, it is necessary to consider both polarization loss and conductivity loss.

In many applications, the dielectric loss must be very low. For instance, in the case of dielectrics used in mm-wave detectors, dielectric losses limit the overall optical efficiency when transferring the mm-wave signal received at the antenna to the detectors [27]. Dielectric losses are also critical for on-chip spectroscopy, as they constrain the quality factor [28]. Among the widely used dielectrics and semiconductors with low losses are SiO_2 [45], SiN_x [46, 47], amorphous Si [48], and silicon carbide [49]. This low loss tangent of 10^{-5} has been observed for a-Si [32] and silicon carbide [33] at microwave frequencies.

On the contrary, when using nanocomposite materials as absorbers of electromagnetic waves, the higher the dielectric loss, the better. The most important properties of the primary material that determine electromagnetic absorption are the imaginary parts of complex permittivity $\varepsilon_r = \varepsilon' - j\varepsilon''$, permeability $\mu_r = \mu' - j\mu''$, and conductivity $\sigma_r = \sigma' - j\sigma''$. However, no materials exhibit high values for all these parameters at all frequencies. Higher values of the loss factor (ε'') will result in a greater attenuation constant, leading to larger attenuation of the electromagnetic wave [34, 35].

Nowadays, a variety of microwave absorption materials are under intensive investigation to create an effective microwave absorber. Among these materials, ferrites, such as ferrospinels and hexaferrites, attract significant research interest due to their high magnetic loss and large Snoek's limit [36]. So far, many ferrite microwave absorbers have been developed, including $ZnFe_2O_4$, $BaFe_{12-x}Al_xO_{19}$ (x = 0.1…1.2), and $Ce(FeTi)O_x$, all of which show great potential in the field of microwave absorption due to their excellent magnetic and dielectric properties. Furthermore, researchers have found that cation substitution can influence the magnetic characteristics and microwave absorption performance of ferrite microwave absorbers [37, 38].

The results on the dielectric losses of alternating electrical signals in nanocomposite Fe_yO_z films are presented in this work. The influence of high-temperature annealing on the dielectric losses of nanocomposite films has been demonstrated. The frequency and voltage dependences of the dielectric losses have been determined. The obtained results are explained in terms of both polarization loss and conductivity loss.

2. Experimental

Nanocomposite Fe_xO_y films were prepared using the ion plasma deposition method [39, 40]. The iron-containing target was used. The deposition was carried out in the atmosphere of argon and oxygen. During the ion-plasma sputtering process, Ar ions knock atoms out of the iron target. The iron atoms are oxidized as they move towards the substrate, and the degree of oxidation depends on the ratio of oxygen to argon gases supplied to the chamber during the sputtering process.

The oxygen content in the gas environment during deposition remained unchanged at 18%. The films were deposited on p-type (100) silicon substrates (ρ = 10 Ω·cm). The deposition was carried out in a vacuum chamber at pressure $P = 6.7\cdot10^{-3}\ldots1\cdot10^{-2}$ Pa, substrate temperature was within 100…120 °C. The thickness of the initial (after deposition) film, determined by laser ellipsometry (λ = 632.8 nm), was 46 nm.

The two types of samples were investigated. One of them is the initial (post-deposition) nanocomposite Fe_xO_y film, while the other is the nanocomposite Fe_xO_y film that was annealed in the Ar atmosphere at T = 1000 °C for 30 minutes.

After the film deposition, Al electrodes were formed on the surface using sputtering through the mask during thermal evaporation. The area of the metal electrodes was $7.85\cdot10^{-3}$ cm^2. The Al contact was also deposited on the backside of the Si wafer. Thus, MIS (Metal–Insulator–Semiconductor) structures were created with the nanocomposite Fe_xO_y film serving as the dielectric.

The dielectric properties of Fe_xO_y films were measured using the Agilent 4294A semiconductor parameter analyzer within the frequency range of 5 kHz to 5 MHz, with the AC measuring signal of 50 mV rms. The variable DC bias up to –20 V (electric field $E = 4.3\cdot10^6$ V/cm) was applied during the impedance spectroscopy measurements. These measurements allowed us to obtain capacitance-voltage (C-V), and tan(δ)-V dependences.

The DC current-voltage characteristics were measured in the dark by using the Keithley 2410 Source Meter.

The analysis of the dielectric parameters was carried out under direct bias, applying a negative voltage to the upper metal electrode of the MIS structure to ensure the accumulation of majority charge carriers (holes) in the near-surface layer of the semiconductor, thereby eliminating the influence of the substrate.

3. Results and discussion

It is well known that dielectric losses are caused by polarization and conductivity and largely depend on the concentration of impurities and structural defects [41]. The value of dielectric losses caused by defects can vary by order of magnitude, while the change in dielectric permittivity may be quite insignificant.

Electromagnetic energy losses and their conversion into thermal energy are characterized by two parameters: the dielectric loss tangent (tan(δ)) and the dielectric loss factor (the imaginary part of the dielectric permittivity, ε″). The dielectric loss tangent is expressed as

$$\tan(\delta) = \tan(90 - \varphi) = \frac{\varepsilon''}{\varepsilon'}, \quad (1)$$

where φ is the phase shift between the voltage and current and ε′ is the dielectric constant (the real part of the dielectric permittivity).

The studied MIS structures are capacitors with parallel plates and a composite dielectric film between them. In this type of capacitor, the capacitance is

$$C = \frac{\varepsilon_0 \varepsilon_r S}{d}, \quad (2)$$

where ε_0 is the vacuum permittivity, ε_r is the dielectric constant, S is the area of the plates, and d is the dielectric thickness.

The experimental capacitance-voltage (C–U) characteristics of the MIS structures with both initial and annealed Fe_xO_y nanocomposite films measured at various frequencies are presented in Fig. 1.

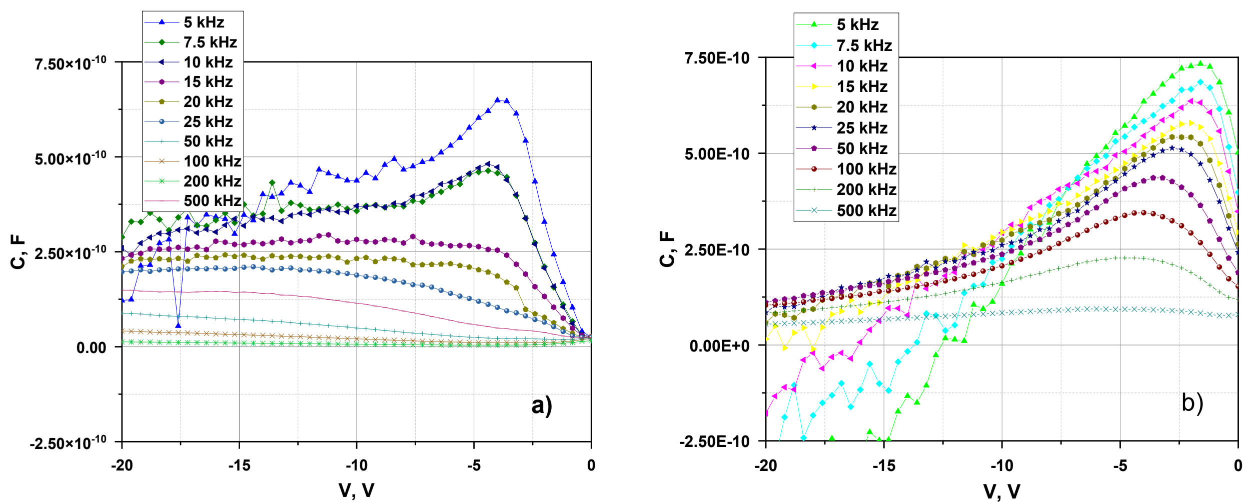

Fig. 1. Capacitance-voltage characteristics of the MIS structures with nanocomposite Fe_xO_y films: a) initial film, b) annealed film. Here and further for the interpretation of the colors, the reader is referred to the web version of this article.

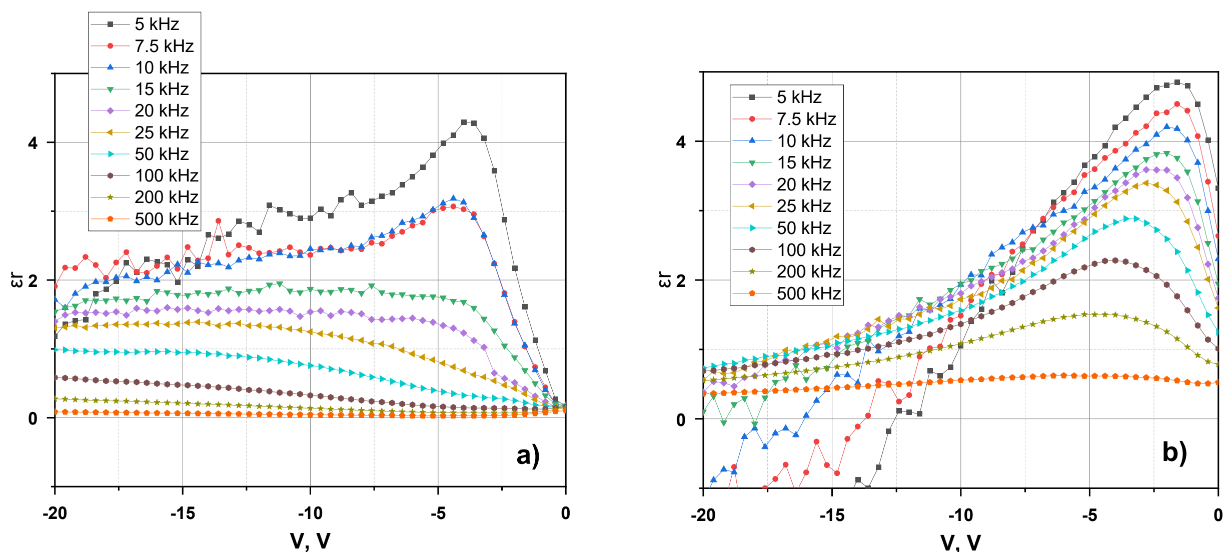

Fig. 2. The dielectric constant dependences on the voltage with the frequency as a parameter: a) initial film, b) annealed film.

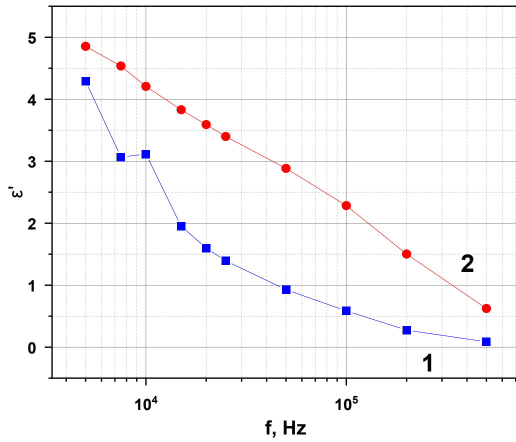

Fig. 3. Frequency dependences of dielectric constant: *1* – initial film, *2* – annealed film.

As can be seen, the behavior of the *C–U* characteristics is quite non-monotonic. Firstly, they increase with increasing voltage, reaching a maximum value before decreasing. This behavior is notably different from that of MIS structures with ideal dielectrics. In the case of structures with ideal dielectrics, the capacitance in the region of surface accumulation of majority carriers remains constant and equal to the capacitance of the dielectric [42]. The decrease in capacitance in this region is caused by the non-ideality of the dielectrics, specifically their relatively high conductivity. We previously observed similar behavior in the *C–U* characteristics of MIS structures nanocomposite films containing Si nanoclusters in a SiO_2 matrix [43] and Au nanoclusters in an Al_2O_3 matrix [44].

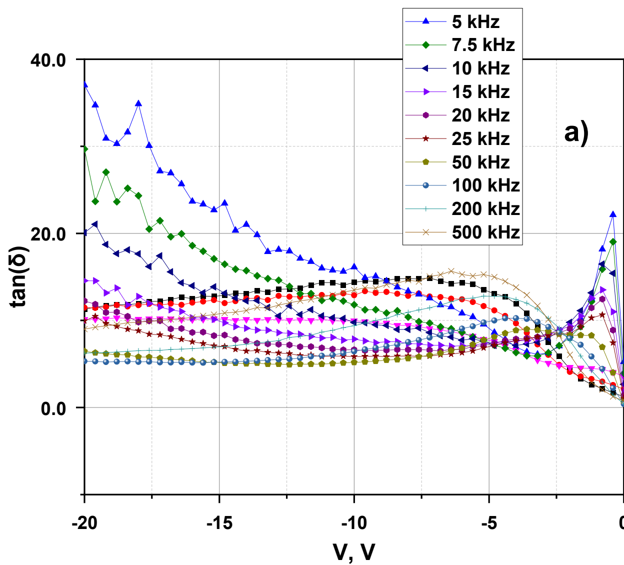

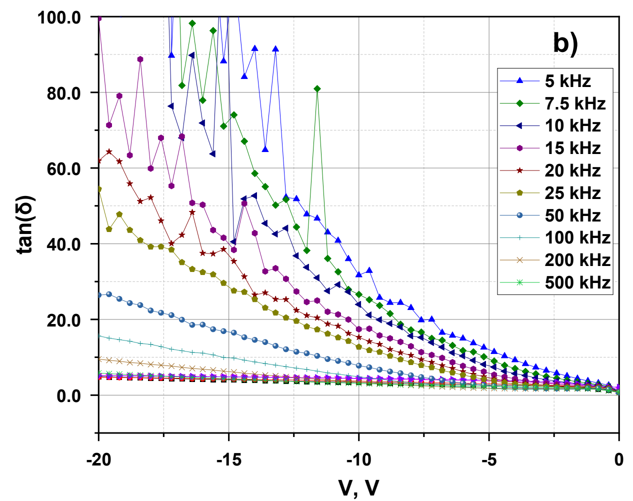

Fig. 4. Dependences of dielectric loss tangent on voltage with frequency as a parameter: a) initial film, b) annealed film.

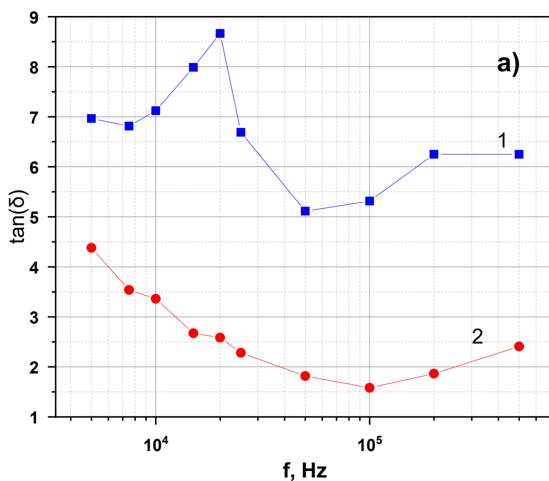

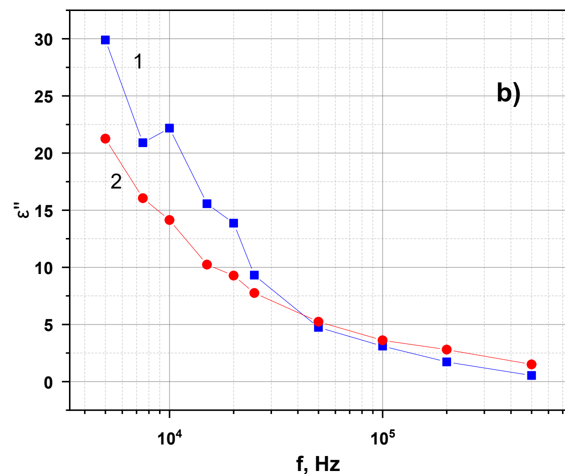

Fig. 5. Dependences of dielectric loss tangent (a) and dielectric loss factor (b) on the frequency: *1* – initial film, *2* – annealed film.

The decrease in the capacitance with frequency is also observed. This behavior is explained by the exclusion of slower polarization mechanisms as frequency increases. A comparison of the *C–U* characteristics of the initial and annealed films shows that the annealed films exhibit higher capacitance. This phenomenon is attributed to the emergence of additional phase interfaces due to structural transformation and, consequently, a more significant influence of the space charge interface Maxwell–Wagner polarization mechanism.

The dielectric constants of the films calculated according to Eq. (2) are shown in Fig. 2. The voltage and frequency behavior of the dielectric constant is similar to that of the *C–U* curves due to the linear relationship between ε_r and C in Eq. (2). As shown in Fig. 2, the obtained values of the dielectric constant are within +5…–1. The frequency dependences of dielectric constant, determined at the voltage corresponding to positive C_{max}, are shown in Fig. 3. The decrease in the dielectric constants is observed for both initial and annealed films. This frequency dependence of the dielectric constant is caused by the suppression of slower polarization mechanisms at higher frequencies due to their inertia. The gradual decrease in the dielectric constant with increasing frequency is characteristic of relaxation (thermally activated) polarization mechanisms [41]. A higher value of dielectric constant is observed for the annealed film, which can be attributed to the transformation of the film structure and some densification during thermal annealing.

The dependences of dielectric loss tangent on the voltage, with frequency as a parameter, are presented in Fig. 4. As can be seen, the dielectric loss tangent in the low voltage region is higher for the initial film, while in the high voltage region – for the annealed one.

The dielectric loss tangent and the dielectric loss factor as functions of frequency, determined at voltages corresponding to positive C_{max}, are shown in Fig. 5. The dielectric loss factor was calculated from the experimental data for the dielectric loss tangent (Fig. 4) and the dielectric constant (Fig. 3) according to Eq. (1).

As shown in Fig. 5a, the frequency dependences of tan(δ) are nonmonotonic, with the higher values for the initial film. It is caused by the ordering of the film structure and the reduction of structural defects. In contrast, the dielectric loss factors monotonically decrease with frequency (Fig. 5b). At lower frequencies, the dielectric loss factor is higher for the initial film, but at higher frequencies, the values are approximately the same for both films.

Another important mechanism of losses in dielectrics is electrical conductivity. The contribution of electrical conductivity to dielectric losses was determined according to the following equation [41, 45, 46]:

$$\varepsilon'' = \frac{\sigma_{dc}}{\omega\varepsilon_0}, \qquad (3)$$

where σ_{dc} is DC electrical conductivity, ε_0 is the permittivity of vacuum, and ω is the frequency.

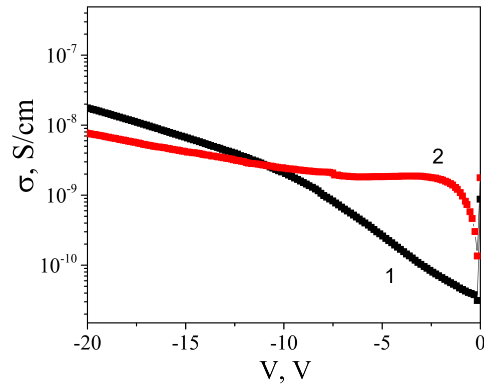

Fig. 6. Dependences of specific conductivity on voltage: *1* – initial Fe_xO_y film, *2* – annealed film.

The specific conductivity of Fe_xO_y nanocomposite films before and after high-temperature annealing are shown in Fig. 6. Based on the obtained results, several conclusions can be drawn: (*i*) the conductivity of the initial film is lower compared to the annealed ones up to the voltage $V \approx 10$ V; (*ii*) at higher voltages ($V > 10$ V)), the conductivity ratio is reversed, meaning that the conductivity of the initial film is higher.

The frequency and voltage dependences of the dielectric loss factor, obtained using Eq. (3), are shown in Fig. 7a, 7b, and 7c, respectively. The dielectric loss factor as a function of frequency was determined at the voltages corresponding to positive C_{max}.

As can be seen in Fig. 7, the dielectric loss factors caused by conductivity are significantly lower compared to those determined from polarization. Dielectric losses due to polarization are predominant. The influence of dielectric losses caused by conductivity increases with voltage (Figs. 7b, 7c). A comparison of the dielectric losses due to conductivity for the initial and annealed films (Figs. 7b, 7c) indicates that, in the lower voltage region, the losses are higher for the annealed film; however, at higher voltages, the dielectric loss factor is greater for the initial film.

Based on the obtained results, we can conclude that the main mechanism of dielectric losses in Fe_xO_y nanocomposite films is due to polarization. For disordered nanocomposite films within the studied frequency range, relaxation (thermally activated) polarization is characteristic. The influence of losses caused by conductivity rises with the increasing applied voltage. Additionally, thermal annealing of the film significantly influences dielectric losses.

In the case of amorphous and nanocomposite films, there are many electron traps in the bandgap [47]. Due to significant structural disorder, these electron traps, caused by lattice defects and impurities, have different atomic environments. As a result, the energy positions of the traps are widely scattered. The existence of the traps in dielectric films significantly influences both polarization and conductivity. The films also contain dipoles.

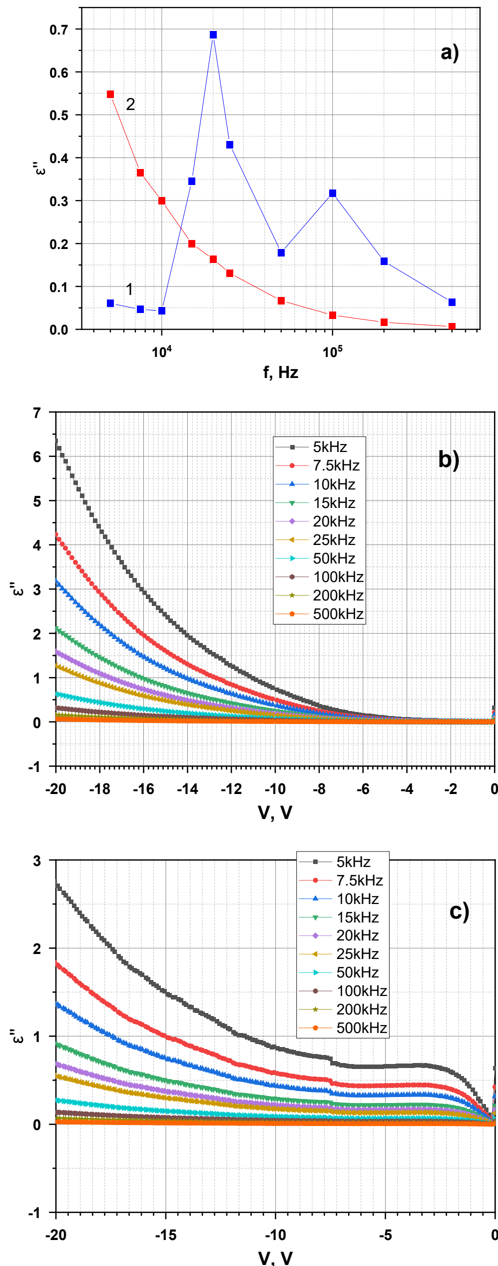

Fig. 7. Frequency (a) and voltage (b, c) dependences of loss factor: a) *1* – initial film, *2* – annealed film, b) initial film, c) annealed film.

The presence of these dipoles in Fe_xO_y films may be caused by dangling Fe-O bonds resulting from differences in the electronegativity of Fe (1.8) and O (3.5) [48]. Relaxation of thermally activated electron and dipole polarizations are characteristic of such disordered films. These polarization mechanisms are relatively slow compared to quasi-elastic polarization [41]. Furthermore, in the case of the annealed films, due to the phase transformation and appearance of additional nano-inclusions of crystalline phase and grain boundaries among nanocrystals and amorphous matrix, the space charge interface Maxwell–Wagner polarization mechanism plays a more significant role.

4. Conclusions

Dielectric losses in Fe_xO_y nanocomposite films were investigated within the frequency range of 5 kHz to 5 MHz. Fe_xO_y films were deposited by ion-plasma sputtering. Impedance spectroscopy and DC measurements were used to determine the dielectric losses. Dielectric losses due to both polarization and conductivity were determined. It was found that dielectric losses due to polarization predominate. Dielectric loss factors due to conductivity are approximately two orders of magnitude lower compared to those determined from polarization. The influence of conduction losses increases with increasing applied DC voltage. In addition, thermal annealing of the film significantly affects the dielectric losses, namely, the losses are lower for the annealed film. The obtained results were explained by the significant role of relaxational thermally activated electronic and dipole polarizations, which are characteristic of disordered nanocomposite films. In the annealed films, due to the phase transformation and appearance of additional nanoinclusions of the crystalline phase and grain boundaries between the nanocrystals and the amorphous matrix, the space charge interface Maxwell–Wagner polarization mechanism plays a more significant role.

Acknowledgements

This research was supported by the National Research Foundation of Ukraine under the project "Development of the technology for mass production of nanocomposite material for the effective absorption of electromagnetic radiation" No. 2025.06/0012.

References

1. Zhong B., Long Z., Yang C. *et al.* Colossal dielectric permittivity in co-doping $SrTiO_3$ ceramics by Nb and Mg. *Ceram. Int.* 2020. **46**. P. 20565–20569. https://doi.org/10.1016/j.ceramint.2020.05.174.
2. Wang D., Zhang S., Wang G. *et al.* Cold sintered $CaTiO_3$-K_2MoO_4 microwave dielectric ceramics for integrated microstrip patch antennas. *Appl. Mater. Today.* 2020. **18**. P. 100519. https://doi.org/10.1016/j.apmt.2019.100519.
3. Somphan W., Thongbai P., Yamwong T. *et al.* High Schottky barrier at grain boundaries observed in $Na_{1/2}Sm_{1/2}Cu_3Ti_4O_{12}$ ceramics. *Mater. Res. Bull.* 2013. **48**. P. 4087–4092. https://doi.org/10.1016/j.materresbull.2013.06.028.
4. Boonlakhorn J., Chanlek N., Manyam J. *et al.* Simultaneous two-step enhanced permittivity and reduced loss tangent in Mg/Ge-doped $CaCu_3Ti_4O_{12}$ ceramics. *J. Alloys Compd.* 2021. **877**. P. 160322. https://doi.org/10.1016/j.jallcom.2021.160322.
5. Lu Z., Bao W., Wang G. *et al.* Mechanism of enhanced energy storage density in $AgNbO_3$-based lead-free antiferroelectrics. *Nano Energy*. 2021. **79**. P. 105423. https://doi.org/10.1016/j.nanoen.2020.105423.

6. Luo B., Wang X., Tian E. *et al.* Giant permittivity and low dielectric loss of Fe doped $BaTiO_3$ ceramics: Experimental and first-principles calculations. *J. Eur. Ceram. Soc.* 2018. **38**. P. 1562–1568. https://doi.org/10.1016/j.jeurceramsoc.2017.10.014.
7. Ramirez A.P., Subramanian M.A., Gardel M. *et al.* Giant dielectric constant response in a copper-titanate. *Solid State Commun.* 2000. **115**. P. 217–220. https://doi.org/10.1016/S0038-1098(00)00182-4.
8. Gong H., Wang X., Zhang S. *et al.* Grain size effect on electrical and reliability characteristics of modified fine-grained $BaTiO_3$ ceramics for MLCCs. *J. Eur. Ceram. Soc.* 2014. **34**. P. 1733–1739. https://doi.org/10.1016/j.jeurceramsoc.2013.12.028.
9. Valant M., Dakskobler A., Ambrozic M. *et al.* Giant permittivity phenomena in layered $BaTiO_3$-Ni composites. *J. Eur. Ceram. Soc.* 2006. **26**. P. 891–896. https://doi.org/10.1016/j.jeurceramsoc.2004.12.034.
10. Manna S., De S.K. Giant dielectric permittivity observed in Li and Zr co-doped NiO. *Solid State Commun.* 2010. **150**. P. 399–404. https://doi.org/10.1016/j.ssc.2009.11.044.
11. Dakhel A.A. Giant dielectric permittivity in Li and Pr co-doped NiO ceramics. *J. Alloys Compd.* 2009. **488**. P. 31–34. https://doi.org/10.1016/j.jallcom.2009.08.155.
12. Havriliak S., Negami S. A complex plane representation of dielectric and mechanical relaxation processes in some polymers. *Polymer* 1967. **8**. P. 161–210. https://doi.org/10.1016/0032-3861(67)90021-3.
13. Maity A., Samanta S., Roy S. *et al.* Giant dielectric constant of copper nanowires/amorphous SiO_2 composite thin films for supercapacitor application. *ACS Omega*. 2020. **5**, No 21. P. 12421–12430. https://doi.org/10.1021/acsomega.0c01186.
14. Evtukh A.A., Kizjak A.Yu., Bratus O.L. Impedance of nanocomposite SiO_2(Si)&Fe_xO_y(Fe) thin films containing Si and Fe nanoinclusions. *SPQEO*. 2023. **26**. P. 424–431. https://doi.org/10.15407/spqeo26.04.424.
15. Kizjak A.Yu., Evtukh A.A., Bratus O.L. *et al.* Electron transport through composite SiO_2(Si)& Fe_xO_y(Fe) thin films containing Si and Fe nanoclusters. *J. Alloys Compd*. 2022. **903**. P. 163892. https://doi.org/10.1016/j.jallcom.2022.163892.
16. Ilchenko V.V., Marin V.V., Vasyliev I.S. *et al.* Admittance spectroscopy using for the determination of parameters of Si nanoclusters embedded in SiO_2. *2014 IEEE 34th Int. Sci. Conf. on Electronics and Nanotechnology (ELNANO)*, 2014. P. 86–89. https://doi.org/10.1109/ELNANO.2014.6873969.
17. Evtukh A., Bratus' O., Ilchenko V. *et al.* Capacitive properties of MIS structures with SiO_x&$Si_xO_yN_z$ films containing Si nanoclusters. *J. Nano Res.* 2016. **39**. P. 162–168. https://doi.org/10.4028/www.scientific.net/JNanoR.39.162.
18. Zhang D., Wang R., Wen M. *et al.* Synthesis of ultralong copper nanowires for high-performance transparent electrodes. *J. Am. Chem. Soc*. 2012. **134**(35). P. 14283–14286. https://doi.org/10.1021/ja3050184.
19. Bhattacharjee S., Banerjee A., Mazumder N. *et al.* Negative capacitance switching in size-modulated Fe_3O_4 nanoparticles with spontaneous non-stoichiometry: Confronting its generalized origin in non-ferroelectric materials. *Nanoscale*. 2020. **12**, No 3. P. 1528–1540. https://doi.org/10.1039/C9NR07902E.
20. Evtukh A., Kizjak A., Bratus O. *et al.* Negative capacitance and dielectric constant of nanocomposite $SiAl_zO_xN_y$ (Si) films with semiconductor nanoparticles. *Nano Lett*. 2024. **24**, No 2. P. 617–622. https://doi.org/10.1021/acs.nanolett.3c03627.
21. Yu T., Zhang S., Xia B., Fu Z. *et al.* A new understanding of dielectric loss in dielectric materials across a wide temperature range. *Ceram. Int.* 2025. **51**. P. 21067–21076. https://doi.org/10.1016/j.ceramint.2025.02.275.
22. Li X., Yang H., Zhu C. *et al.* Enhanced high-temperature energy storage properties in BNT-based ceramics with well-controlled low dielectric loss. *Ceram. Int.* 2024. **50**. P. 1438–1442. https://doi.org/10.1016/j.ceramint.2023.10.233.
23. Mantas P.Q. Dielectric response of materials: extension to the Debye model. *J. Eur. Ceram. Soc.* 1999. **19**. P. 2079–2086. https://doi.org/10.1016/S0955-2219(98)00273-8.
24. Cai E., Peng S., Liu Q. Superior piezoelectricity in lead-free barium titanate piezoceramics. *J. Materiomics*. 2024. **10**. P. 694–706. https://doi.org/10.1016/j.jmat.2023.09.006.
25. Qin M., Zhang L., Wu H. Dielectric loss mechanism in electromagnetic wave absorbing materials. *Adv. Sci*. 2022. **9**, No 10. P. 2105553. https://doi.org/10.1002/advs.202105553.
26. Fan J., He G., Long Z. *et al.* High insulation resistivity and low dielectric loss in (Ta, Al)-codoped $BaTiO_3$ colossal permittivity materials. *J. Am. Ceram. Soc.* 2024. **107**. P. 4854–4863. https://doi.org/10.1111/jace.19775.
27. Abitbol M.H., Ahmed Z., Barron D. et al. *CMB-S4 Technology Book*, 2017. https://doi.org/10.48550/arXiv.1706.02464.
28. Hailey-Dunsheath S., Shirokoff E., Barry P.S. *et al.* Status of SuperSpec: a broadband, on-chip millimeter-wave spectrometer. *Proc. SPIE.* 2014. **9153**. id. 91530M. https://doi.org/10.1117/12.2057229.
29. Pan Z., Barry P.S., Cecil T. *et al.* Measurement of dielectric loss in silicon nitride at centimeter and millimeter wavelengths. *IEEE Trans. Appl. Superconduct.* 2023. **33**, No 5. P. 1101707. https://doi.org/10.1109/TASC.2023.3264953.
30. Ye Z., Fülöp A., Helgason Ó.B. *et al.* Low-loss high-Q silicon-rich silicon nitride microresonators for Kerr nonlinear optics. *Opt. Lett*. 2019. **44**, No 13. P. 3326. https://doi.org/10.1364/OL.44.003326.
31. Paik H., Osborn K. D. Reducing quantum-regime dielectric loss of silicon nitride for superconducting quantum circuits, *Appl. Phys. Lett.* 2010. **96**, No. 7. https://doi.org/10.1063/1.3309703.

32. Defrance F., Shu S., Beyer A. *et al.* Low intrinsic TLS loss in hydrogenated amorphous silicon. *SPIE* XI. 2022. P. PC121900D. https://doi.org/10.48550/arXiv.2412.09693.
33. Buijtendorp B.T., Vollebregt S., Karatsu K. *et al.* Hydrogenated amorphous silicon carbide: A low-loss deposited dielectric for microwave to submillimeter wave superconducting circuits. *Phys. Rev. Appl*. 2022. **18**, No 6. P. 064003. https://doi.org/10.1103/PhysRevApplied.18.064003v.
34. Elmahaishi M.F., Azis R.S., Ismail I., Muhammad F.D. A review on electromagnetic microwave absorption properties: their materials and performance. *J. Mater. Res. Technol*. 2022. **20**. P. 2188–2220. https://doi.org/10.1016/j.jmrt.2022.07.140.
35. Liang H., Xing H., Qin M., Wu H. Bamboo-like short carbon fibers@Fe_3O_4@phenolic resin and honeycomb-like short carbon fibers@Fe_3O_4@FeO composites as high-performance electromagnetic wave absorbing materials. *Compos. A: Appl. Sci. Manuf.* 2020. **135**. P. 105959. https://doi.org/10.1016/j.compositesa.2020.105959.
36. Tartaj P., Serna C.J. Synthesis of monodisperse superparamagnetic Fe/silica nanospherical composites. *J. Am. Chem. Soc.* 2003. **125**, No 51. P. 15754–15755. https://doi.org/10.1021/ja0380594.
37. Ebrahimi-Tazangi F., Hekmatara S.H., Seyed-Yazdi J. Remarkable microwave absorption of GO-SiO_2/Fe_3O_4 via an effective design and optimized composition. *J. Alloys Compd*. 2021. **854**. P. 157213. https://doi.org/10.1016/j.jallcom.2020.157213.
38. Jaiswal R., Agarwal K., Pratap V. *et al.* Microwave-assisted preparation of magnetic ternary core-shell nanofiller ($CoFe_2O_4$/rGO/SiO_2) and their epoxy nanocomposite for microwave absorption properties. *Mater. Sci. Eng.: B*. 2020. **262**. P. 114711. https://doi.org/10.1016/j.mseb.2020.114711.
39. Kelsall R.W., Hamley I.W., Geoghegan M. (Eds.) *Nanoscale Science and Technology*. John Wiley & Sons, Ltd, 2005. https://doi.org/10.1002/0470020873.
40. Bratus O.L., Evtukh A.A., Lytvyn O.S. *et al.* Structural properties of nanocomposite SiO_2(Si) films obtained by ion-plasma sputtering and thermal annealing. *SPQEO.* 2011. **14**. P. 247–255. https://doi.org/10.15407/spqeo14.02.247.
41. Poplavko Yu.M. *Electronic Materials: Principles and Applied Science*. Elsevier Inc., 2019. https://doi.org/10.1016/C2017-0-03281-0.
42. Sze S.M., Li S., Ng K.K. *Physics of Semiconductor Devices*. John Wiley & Sons, Ltd, 2021.
43. Begun E.V., Bratus' O.L., Evtukh A.A. *et al.* Charge characteristics of the MOS structures with oxide films containing Si nanocrystals. *SPQEO.* 2007. **10**. P. 46–50. https://doi.org/10.15407/spqeo10.02.046.
44. Bratus' O., Evtukh A., Kaganovich E. *et al.* Charge storage characteristics of gold nanoparticles embedded in alumina matrix. *SPQEO.* 2009. **12**. P. 53–56. https://doi.org/10.15407/spqeo12.01.053.
45. Evtukh A.A., Antonin S.V., Pylypov A.I. *et al.* Dielectric losses in SiO_x&Fe_yO_z(Fe) nanocomposite films. *SPQEO.* 2025. **28**. P. 175–182. https://doi.org/10.15407/spqeo28.02.175/
46. Ilyas M., Zulfequar M., Husain M. Anomalous dielectric behaviour in a-Ga_xTe_{100-x} alloys ($0 \le x \le 10$). *Phys. B: Condens. Matter.* 1999. **271**. P. 125–135. https://doi.org/10.1016/S0921-4526(99)00221-5.
47. Mott N.F., Davis E.A. *Electron Processes in Non-crystalline Materials*. Clarendon Press, Oxford, 1979.
48. Pauling F., Pauling P. *Chemistry.* W.H. Freeman and Company, San Francisco, 1975.

Authors' contributions

Evtukh A.A.: key ideas, conceptualization, analysis, validation, supervision, writing – review & editing.
Pypypov A.I.: investigations, initial draft preparation, writing.
Muryi Y.U.: investigations, results analysis.
Pypypova O.V.: conductivity measurements, investigations, analysis.
Antonin S.V.: impedance measurements, investigations, analysis.
Bratus O.L.: film deposition and characterization, investigations.

Authors and CV

Anatoliy Evtukh, Doctor of Sciences in Physics and Mathematics, Professor, Head of the Department of Physics of Surface and Nanophotonics, V. Lashkaryov Institute of Semiconductor Physics, NAS of Ukraine. Authored over 300 publications. His main research activity is in the field of nanomaterials and nanostructures, composite films with semiconductor and metal nanoinclusions, electron transport, microwave absorption, surface physics, semiconductor technologies, sensors, and solar cells.
https://orcid.org/0000-0003-3527-9585

Anton Pylypov, PhD student at the Taras Shevchenko National University of Kyiv, Educational and Research Institute of High Technologies. The area of his scientific interests includes physics and technology of semiconductor materials, electronics devices and sensors (photoresistors, light-emitted structures, *etc.*), as well as the analysis, diagnostics, modeling, and forecasting of physical processes in different objects, knowledge of circuitry, electronics, and modern element base.
E-mail: pylypov.anton@gmail.com,
https://orcid.org/0009-0009-2996-1503

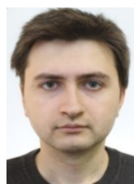

Yaroslav Muryi defended his PhD in applied physics and nanomaterials in 2024. Junior researcher at the V. Laskaryov Institute of Semiconductor Physics, NASU. The area of scientific fields includes nanomaterials and nanostructures, composite films, interaction of electromagnetic waves with matter, and semiconductor technologies. E-mail: muryi@ukr.net, https://orcid.org/0000-0001-5107-0138

Serhii Antonin defended his PhD thesis in applied physics and nanomaterials in 2022. Researcher at the V. Lashkaryov Institute of Semiconductor Physics, NAS of Ukraine. The area of scientific interests includes nanomaterials and nanostructures, composite films, semiconductor technologies, and solar cells. E-mail: antoninsv@gmail.com, https://orcid.org/0000-0003-1607-9721

Olha Pylypova, PhD, Assistant Professor at the Taras Shevchenko National University of Kyiv, Educational and Research Institute of High Technologies. Authored over 69 publications and 2 textbooks. The area of her scientific interests includes physics and technology of semiconductor materials, such as SiO_x and hybrid structures and devices (solar cells, photoresistors, light-emitted structures, *etc.*), as well as the analysis, diagnostics, modeling and forecasting of physical processes in different objects. E-mail: olha.pylypova@knu.ua, https://orcid.org/0000-0002-0337-4724

Oleh Bratus, Doctor of Sciences in Physics and Mathematics (Physics of Solid States), Senior Researcher at the Department of Physics of Surface and Nanophotonics, V. Lashkaryov Institute of Semiconductor Physics, NAS of Ukraine. Authored over 80 publications. His main research activity is in the field of semiconductor technologies, nanomaterials and nanostructures, composite films with semiconductor and metal nanoinclusions, electron transport, surface physics, and solar cells.
E-mail: o.l.bratus@gmail.com,
https://orcid.org/0000-0002-2661-6482

Особливості діелектричних втрат у нанокомпозитних плівках Fe_xO_y

А.А. Євтух, А.І. Пилипов, Я.Ю. Мурий, О.В. Пилипова, С.В. Антонін, О.Л. Братусь

Анотація. Діелектричні втрати є одним з основних параметрів діелектрика. Як правило, для багатьох застосувань вони повинні бути якомога нижчими, однак у випадку поглинання електромагнітних хвиль вони повинні бути високими. У цій статті наведено результати дослідження діелектричних втрат у нанокомпозитних плівках Fe_xO_y, які досліджувалися в діапазоні частот від 5 кГц до 5 МГц. Було продемонстровано, що діелектричні втрати, спричинені прикладеним сигналом змінного струму, зменшуються з частотою та зростають з напругою. Аналіз механізмів діелектричних втрат показав, що вони, в першу чергу, спричинені поляризацією. Діелектричні втрати, спричинені провідністю, були приблизно на два порядки меншими, хоча вони значно зростають зі збільшенням прикладеної напруги. Ця поведінка корелює із залежністю питомої провідності від напруги. Тангенс кута діелектричних втрат (tan δ) та коефіцієнт діелектричних втрат (уявна частина діелектричної проникності, ε′′) вищі для вихідної плівки порівняно з відпаленою. Цю різницю можна пояснити трансформацією структури плівки та її впорядкуванням під час високотемпературного термічного відпалу. Загалом, діелектричні втрати в досліджуваному діапазоні частот в основному спричинені релаксаційною (термічно активованою) поляризацією, яка характерна для невпорядкованих нанокомпозитних плівок.

Ключові слова: нанокомпозитні плівки, діелектричні втрати, поляризація, частота, напруга, іонно-плазмове осадження, відпал.